Journal of the Mechanical Behavior of Biomedical Materials 90 (2019) 451–459

Contents lists available at ScienceDirect

Journal of the Mechanical Behavior of Biomedical Materials

journal homepage: www.elsevier.com/locate/jmbbm

Designed for resistance to puncture: The dynamic response of fish scales

S. Ghods[a], S. Murcia[a], E.A. Ossa[b], D. Arola[a,c,*]

[a] Department of Materials Science and Engineering, University of Washington, Seattle, WA, USA
[b] School of Engineering, Universidad EAFIT, Medellín, Colombia
[c] Department of Mechanical Engineering, University of Washington Seattle, WA, USA

ARTICLE INFO

Keywords:
Bioinspiration
Fish scales
Natural armor
Puncture
Strain rate
Toughness

ABSTRACT

Natural dermal armors are serving as a source of inspiration in the pursuit of "next-generation" structural materials. Although the dynamic strain response of these materials is arguably the most relevant to their performance as armors, limited work has been performed in this area. Here, uniaxial tension and transverse puncture tests were performed on specimens obtained from the scales of Asian carp over strain rates spanning seven decades, from 10^{-4} to 10^{3} s^{-1}. The importance of anatomical variations was explored by comparing the performance of scales from the head, middle and tail regions. In both loading orientations, the scales exhibited a significant increase in the resistance to failure with loading rate. The rate sensitivity was substantially higher for transverse loading than for in-plane tension, with average strain rate sensitivity exponents for measures of the toughness of 0.35 and 0.08, respectively. Spatial variations in the properties were largest in the puncture responses, and scales from the head region exhibited the greatest resistance to puncture overall. The results suggest that the layered microstructure of fish scales is most effective at resisting puncture, rather than in-plane tension, and its effectiveness increases with rate of loading. X-ray microCT showed that delamination of plies in the internal elasmodine and stretching of the fibrils were key mechanisms of energy dissipation in response to puncture loading. Understanding contributions from the microstructure to this behavior could guide the development of flexible engineered laminates for penetration resistance and other related applications.

1. Introduction

Interest in the science of natural structural materials has been expanding for over a decade now (Currey, 1999; Mayer, 2006; Meyers et al., 2011; Barthelat, 2013). One category of materials that has attracted substantial interest is flexible dermal armors (Yang et al., 2013a). These materials are charged with providing protection against physical threats, and are subjected to the most extreme loading conditions. The dermal armors of armadillo (Chen et al., 2011), alligators and crocodiles (Achrai and Wagner, 2013; Sun and Chen, 2013; Chen et al., 2014), the pangolin (Wang et al., 2016), turtles (Chen et al., 2015; Chang and Chen, 2016), and fish (Ikoma et al., 2003; Bruet et al., 2008; Torres et al., 2008; Lin et al., 2011; Yang et al., 2013b) are materials being explored in this area; they provide protection over a large range in flexibility, with fish scales being the most flexible overall. Based on their morphology, the armors of the aforementioned animals appear unique, but all are biological composites and composed of organic and inorganic building blocks that are organized with a hierarchical structure (Wegst et al., 2015). What potentially sets these armors apart from one another is the organization of the constituents into specific structural elements at larger length scales, which are considered important for tuning the mechanical behavior (Naleway et al., 2015).

Fish scales are of particular interest in the most recent pursuits to develop bioinspired materials (Browning et al., 2013; Zhu et al., 2013; Chintapalli et al., 2014; Rudyk et al., 2015; Martini and Barthelat, 2016). The scales in modern fish have evolved into four primary groups including cosmoid, placoid, ganoid and elasmoid scales (Sire and Huysseune, 2003; Kardong, 2006). Scales of the first three groups are all relatively rigid in comparison to elasmoid scales, which results from their larger thickness and the presence of bony regions with much higher mineral content (Sherman et al., 2017). Flexibility in these dermal armors is achieved by the way the scales articulate with respect to one another, rather than the flexibility of the scales themselves. In comparison to the other three scale types, elasmoid scales are much thinner, and are stacked or overlayed with respect to one another to facilitate flexibility and protection simultaneously. Elasmoid scales are characteristic of fish with greater speed, and could be considered more multi-functional as their flexibility appears to be equally important to the puncture resistance (Bruet et al., 2008; Jandt, 2008). For that

* Correspondence to: Department of Materials and Engineering, University of Washington, Roberts Hall, 333, Box 352120, Seattle, WA 98195-2120, USA.
E-mail address: darola@uw.edu (D. Arola).

https://doi.org/10.1016/j.jmbbm.2018.10.037
Received 29 October 2017; Received in revised form 25 May 2018; Accepted 30 October 2018
Available online 02 November 2018
1751-6161/

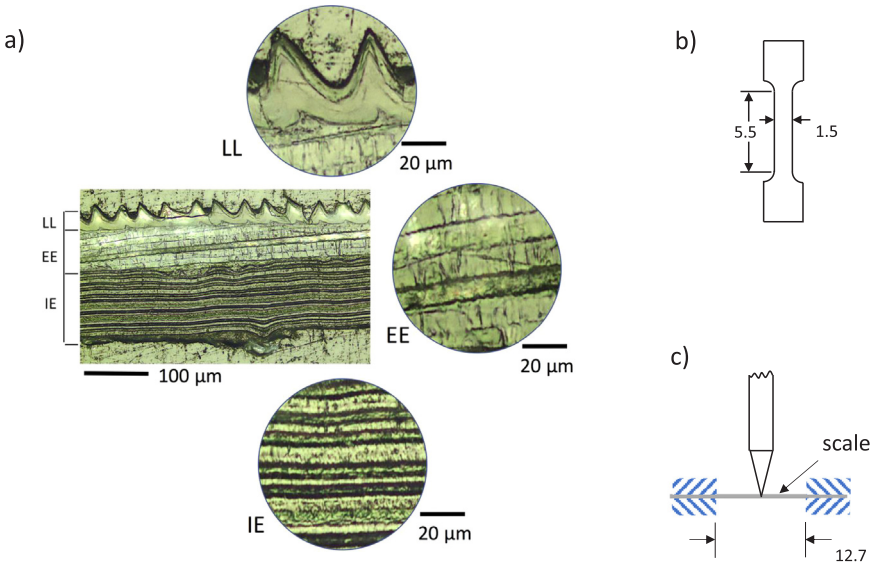

Fig. 1. Details of the scales and the experimental methods adopted for evaluating the dynamic behavior. a) carp scale cross-sections for representative head and tail scales. The three principal layers are highlighted including the limiting layer (LL), external elasmodine (EE) and internal elasmodine (IE), b) tensile testing specimen, b) puncture testing schematic. The scales were clamped circumferentially around the boundary of the central exposed section. All units are in millimeters.

reason, they are an excellent system to study and learn from.

The primary building blocks of elasmoid scales are apatite and type I collagen fibers (Lin et al., 2011; Garrano et al., 2012; Zhu et al., 2012; Gil-Duran et al., 2016). The microstructure of these scales consists of two primary layers, including a thin outermost highly mineralized layer, and the elasmodine layer, which occupies the bulk of the thickness. The outermost layer, known as the Limiting Layer (LL), is a highly-mineralized matrix of calcium-deficient apatite crystals reinforced by a sparse dispersion of thin collagen fibers (Zylberberg, 1985). The elasmodine layer consists of a number of lamina (or plies) of unidirectional type I collagen fibrils. Closer scrutiny shows that the elasmodine layer actually consists of two discrete layers, the external and internal elasmodine (Murcia et al., 2015), that are differentiated by the relative mineral content (Fig. 1a). The internal elasmodine (IE) consists of discrete plies of unidirectional collagen fibers with little to no mineral reinforcement. The external elasmodine (EE) exhibits higher mineral content than the IE, but far less than the LL (Murcia et al., 2016). The plies of the entire elasmodine are arranged in the form of a plywood structure (i.e. a lamination of unidirectional fiber layers with rotation between plys), with rotation between plies ranging between 60° and 90° depending on the fish (Bigi et al., 2001). For the carp, the average angle of rotation between plies is 75° (Murcia et al., 2017).

The strong mineral gradient across the thickness of elasmoid scales results in distinct spatial variations in the hardness and elastic modulus. From the limiting layer to the internal elasmodine there is a reduction in elastic modulus and hardness (Lin et al., 2011), which reportedly plays an important role on the puncture resistance (Zhu et al., 2012). Due to the high mineral content, the LL dissipates energy by brittle fracture. The failure process continues to the EE, which results in delamination at the LL/EE interface, as well as between adjacent plies. Once the LL and EE have undergone gross failure, further penetration is resisted by stretching of fibrils of the IE plies, as well as rotation and delamination along the interface of the collagen plies (Zimmerman et al., 2013; Yang et al., 2014). The combination of delamination, rotation of the plies and inelastic deformation of the individual lamina provides the scales with incredible notch insensitivity (Khayer Dastjerdi and Barthelat, 2015) and resistance to fracture (Yang et al., 2014). Due to its composition and the aforementioned mechanisms of deformation, the IE contributes substantially to the toughness, and over a large range of temperatures (Murcia et al., 2015).

Flexible or “wearable” armor materials require low stiffness and high resistance to puncture. As the scaled dermal armor of fish exhibit flexibility, and their structure appears to be developed for protection, the puncture resistance of scales has received considerable attention (e.g. Zhu et al., 2012, 2013; Meyers et al., 2012; Allison et al., 2013; Khayer Dastjerdi and Barthelat, 2015). But while the dynamic response of these materials is one of the most relevant to their performance to resist attack, limited work has addressed the properties of scales under dynamic loading. In fact, only a single study has performed an evaluation of the strain rate dependence of fish scale properties, which was performed in uniaxial tension (Lin et al., 2011). Owing to the importance of interfaces in natural structural materials (Barthelat et al., 2016), and the different mechanisms they impart to the structural behavior, the strain rate dependence of scales and their resistance to failure could be quite different in the axial and transverse loading arrangements. The interfaces may contribute to the transmission of damage differently in transverse puncture and tension, simply by virtue of the stress state and the interface orientations.

In this investigation, the dynamic loading response of fish scales was evaluated in uniaxial tension and transverse puncture to failure. The primary objective was to characterize the importance of the layered microstructure on the strain rate sensitivity of the deformation behavior and its orientation dependence.

2. Materials and methods

Scales of the *Cyprinus carpio* (i.e. the common freshwater carp) were obtained by extraction from across the body of several fish. The fish were purchased from a commercial vendor and marketed as East Asian carp. They were selected to ensure that the weight, number of scales along the lateral nerve line, and microstructure of the scales were consistent amongst the fish analyzed. The scales were obtained nearly equidistant between the ventral and dorsal aspects of the body (i.e. adjacent to the midline) and from three regions including near the head, mid-length (beneath the dorsal fin) and near the tail. To be consistent, these regions were defined at distances from the gill plate of approximately 15%, 40% and 80% of the total number of scales counted along the lateral line over the fish length. Thus, 15% represents at the point that is 15% of the total distance from the gill plate to the last row of scales, and so on. All of the scales were less than 1 mm thick and possessed a diameter that varied according to the anatomical position, with reduction from near the head to the tail. The effective diameter of all scales was greater than 1 cm. After extraction, the scales were stored in Hanks Balanced Salt Solution (HBSS) at 3–5 °C for less than one month to minimize the possibility of degradation.

To support an evaluation of the tensile properties, conventional dog-bone shaped tensile specimens were sectioned from the scales using a punch and stamping process (Garrano et al., 2012). A single specimen

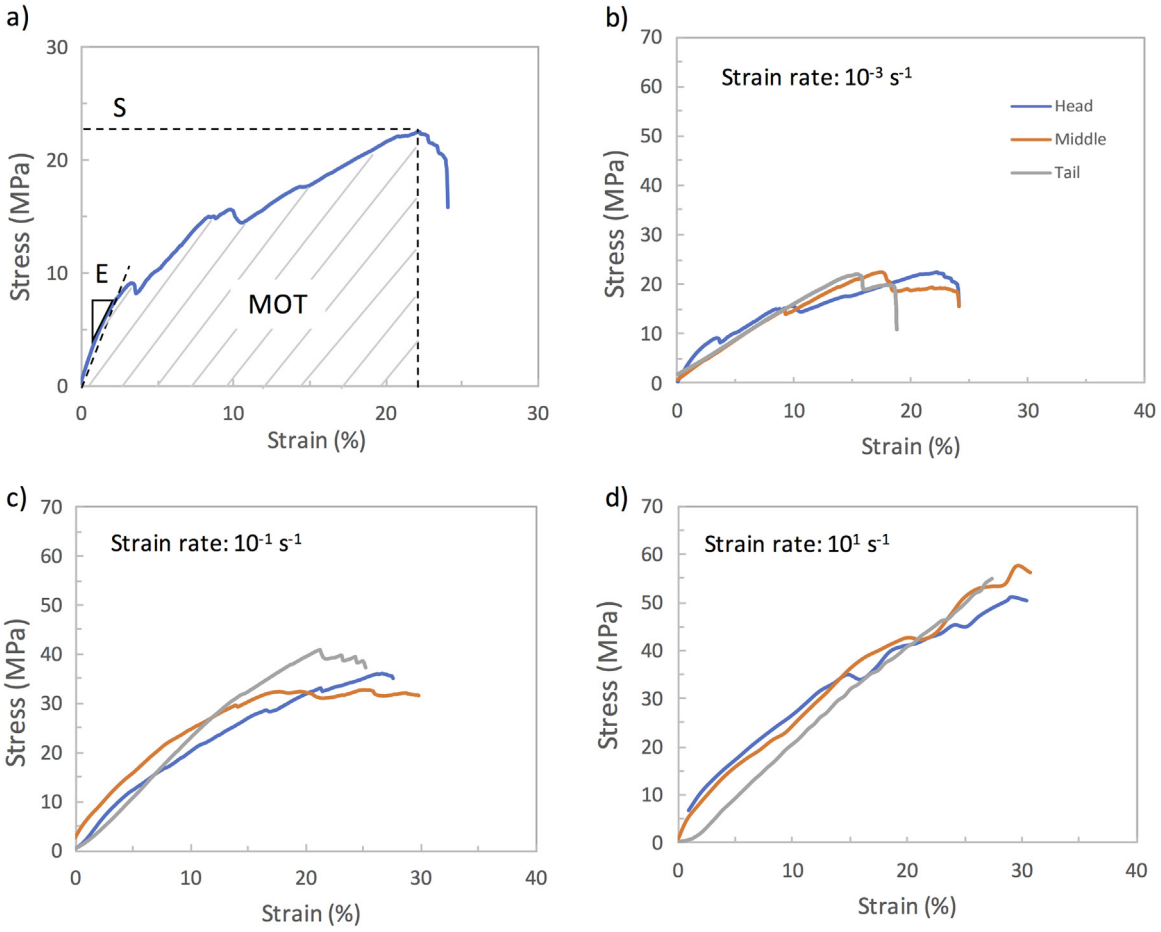

Fig. 2. Representative stress-strain responses for scales from the three representative regions at three different strain rates. a) response for a scale from the head region and definition of the measured properties. E, S and MOT represent the elastic modulus, strength and modulus of toughness, respectively. b) 10^-3 s^-1, c) 10^-1 s^-1, and d) 10^1 s^-1 strain rates.

was stamped from the center region of each scale where the thickness is most uniform. The specimens possessed a gage section length of 5.5 mm and 1.5 mm, respectively, as shown in Fig. 1b. All of the specimens were obtained with alignment parallel to the fish length, for consistency, as scales from the head region can exhibit anisotropic behavior (Murcia et al., 2015). After sectioning, the specimens were returned to the HBSS bath at 3–5 °C.

Tensile testing of the hydrated fish scale specimens was performed to failure at room temperature. The loading was performed under displacement control using a commercial universal testing machine (Instron ElectroPuls E1000, MA) equipped with load cell having full-scale range of 250 N and load precision of 0.01%. Stroke rates were selected to obtain strain rates from 1×10^{-4} to $1 \times 10^{2}\,s^{-1}$ in decades, which were estimated according to the specimen gage length. All specimens were tested to failure. Five specimens were evaluated for each strain rate and anatomical region (head, middle and tail), which resulted in 7 rates x 3 regions x 5 specimens = 105 total tests.

The elastic modulus (E), strength (S) and modulus of toughness (MOT) were determined from results of the tension tests at each rate using the engineering stress-strain definitions. The elastic modulus was determined using the tangent method for strains less than 1% and the strength was defined by the maximum stress realized by the sample. The modulus of toughness was calculated by integrating the area under the stress-strain curves as a function of strain until failure.

Puncture tests were conducted on specimens from the three anatomical regions (Fig. 1a) using a sharp stainless steel punch with tip radius of curvature of 40 μm and included angle of 30°. Loading was conducted using a universal testing machine (Model ELF 3300, BOSE, Eden Prairie, MN, USA) on scales clamped within a dedicated fixture at rates that ranged from 5×10^{-2} to 50 mm/s. The scales were unsupported and clamped around the periphery with exposed portion of 12.5 mm as shown in Fig. 1c. With an average scale thickness of approximately 0.5 mm, and ignoring the out of plane deflection, the loading rates corresponded to strain rates of approximately 1×10^{-1} to $1 \times 10^{3}\,s^{-1}$. Of note, the actual strain rates for the puncture tests varied according to the scale thickness. In all testing the scales were arranged with limiting layer oriented towards the punch and the load and displacement were acquired at a rate of 4 kHz. The scale performance was evaluated in terms of the maximum punch load as well as the work to puncture, which was obtained by integrating the load load-line displacements to the point of maximum load. For both the tension and puncture loading formats, validation tests were performed using specimens prepared from a polycarbonate sheet of 0.38 mm thickness, which is comparable to that of the scales.

The microstructure of scales within each region of evaluation was examined using scanning electron microscopy (JEOL, Model JSM-6010PLUS/LA, Peabody, MA). The samples were sputtered with Au/Pd and observed in secondary electron imaging mode. In addition, selected scales were evaluated after puncture testing using microCT scanning with a North Star Imaging X5000. For this effort, the scales were treated with a very light coating of diluted ethylene glycol after Ryou et al. (2013) to maintain the moisture content within the scale and to minimize any distortion related to dehydration during scanning. Scales from the head region that were subjected to puncture loading at a loading rate of 50 mm/s were scanned using the microCT. The scans were performed using 50 kV and 1000 uA, 1 frame/sec step scan mode with

10 ms delay, 900 projections, and two frame averaging. These conditions were identified as most appropriate for evaluating the scales according to a series of preliminary studies. Based on the fixture arrangement used, x-ray source and detector positioning, a geometric zoom of approximately 50x was achieved, which resulted in a resolution of 3 μm/pixel. Radiographs were treated using the systems imaging software (efX-CT, Version 1.6, North Star Imaging, Rogers, MN, USA) to obtain images of relevance for display.

3. Results

Typical stress-strain diagrams resulting from the uniaxial tension tests are shown in Fig. 2. A single response obtained from the scale of the tail region at a rate of $1 \times 10^{-3}\ s^{-1}$ is shown in Fig. 2a. The elastic modulus (E), strength (S) and modulus of toughness (MOT) are highlighted for reference. These measures were used as metrics for characterizing the tensile responses of all the scale samples tested. Representative responses obtained at low, intermediate and high loading rates (1×10^{-3}, 1×10^{-1} and 1×10^{1}, respectively) are in shown in Fig. 2b through d, respectively. These graphs include responses obtained for scales from each of the three regions of the fish. As evident from the responses at the three strain rates, there is an increase in the strength and the degree of inelastic deformation to failure with increasing loading rate.

The contribution of loading rate to the elastic modulus, strength, strain to failure and modulus of toughness of the scales is shown in Fig. 3a through d, respectively. The data in each graph presents the average and standard deviation of responses obtained for the three regions of evaluation, namely the head, middle and tail. Although there is an increase in all four properties with loading rate, the trends are not the same in each of the properties. For instance, the elastic modulus underwent the largest increase in magnitude (up to 3 ×) over the range in strain rate as evident in Fig. 3a. The smallest increase with loading rate was found in the strain to fracture, with approximately 1.5X increase over the range of loading rate (Fig. 3c).

The strain rate sensitivity of the scales was interpreted from the measures of toughness for each of the three regions. While not a traditional property to evaluate the rate sensitivity, the toughness measurement accounts for the changes in both the strength and the degree of inelastic deformation to failure. A power law was used to quantitatively characterize the responses according to $MOT = A\dot{\varepsilon}^m$, with a coefficient (A) and sensitivity exponent (m). In tension, the values of m for the head, middle and tail were 0.06, 0.07 and 0.08, respectively.

A representative load vs displacement response for transverse loading to puncture of the scales is shown in Fig. 4a. Note that the stiffness, max load to puncture and corresponding work to maximum load were used to quantify the mechanical behavior for this loading condition. Representative puncture responses for selected low, intermediate and high loading rates are shown in Fig. 4b through d, respectively; each of these graphs include typical responses for the three regions of evaluation as well as responses for the polycarbonate (PC) control. Consistent with the responses in tension, there was an increase in resistance to failure with increasing loading rate (Fig. 3d). However, in contrast to the increase in extensibility of the scales with loading rate in tension, the deformation to puncture decreased with loading rate as evident from comparing the responses from Fig. 4b through d.

A clearer view of the influence from loading rate on the puncture resistance of the scales is shown in Fig. 5. Specifically, individual responses for the stiffness, max load and work to puncture are presented in Fig. 5a through c, respectively, as a function of loading rate. Results

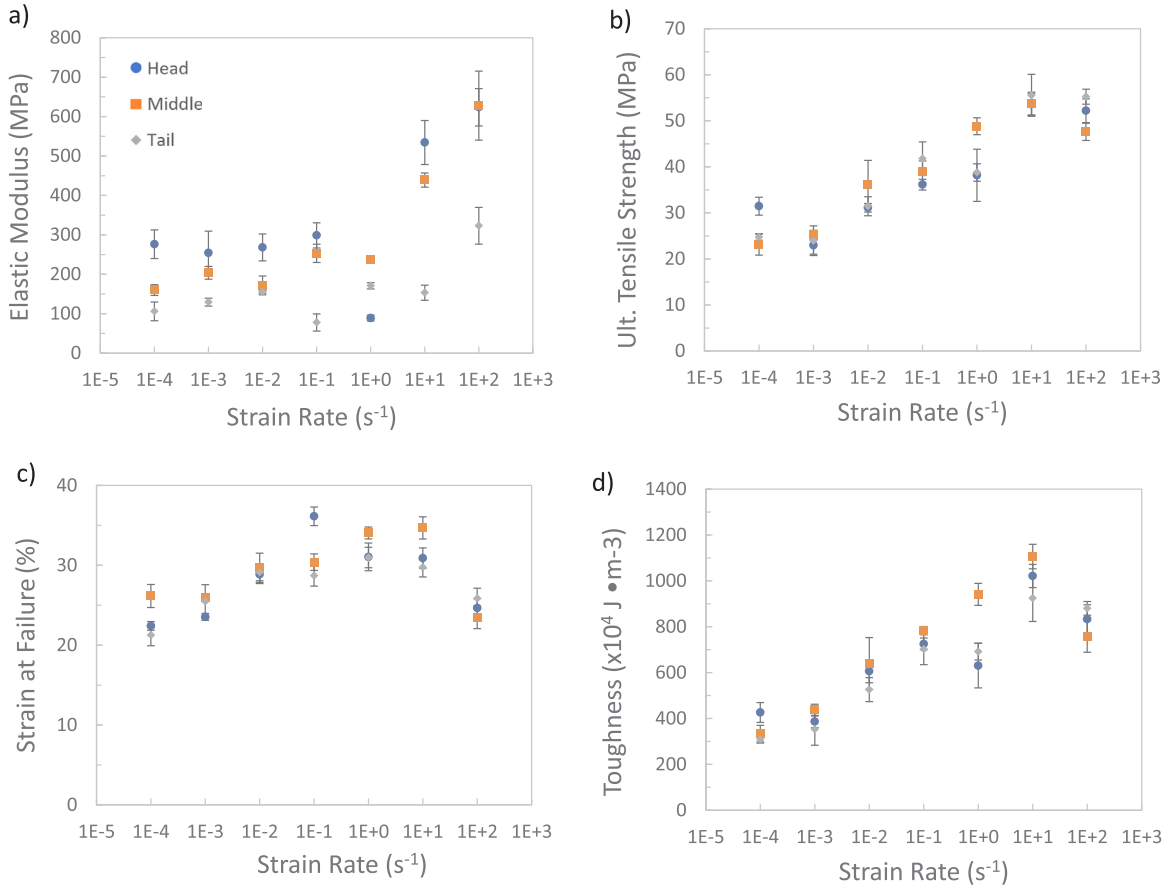

Fig. 3. Strain rate dependence in the tensile responses of the scales for each of the three regions. (a) elastic modulus (E), (b) ultimate tensile strength (S), (c) strain at failure, and (d) modulus of toughness (MOT).

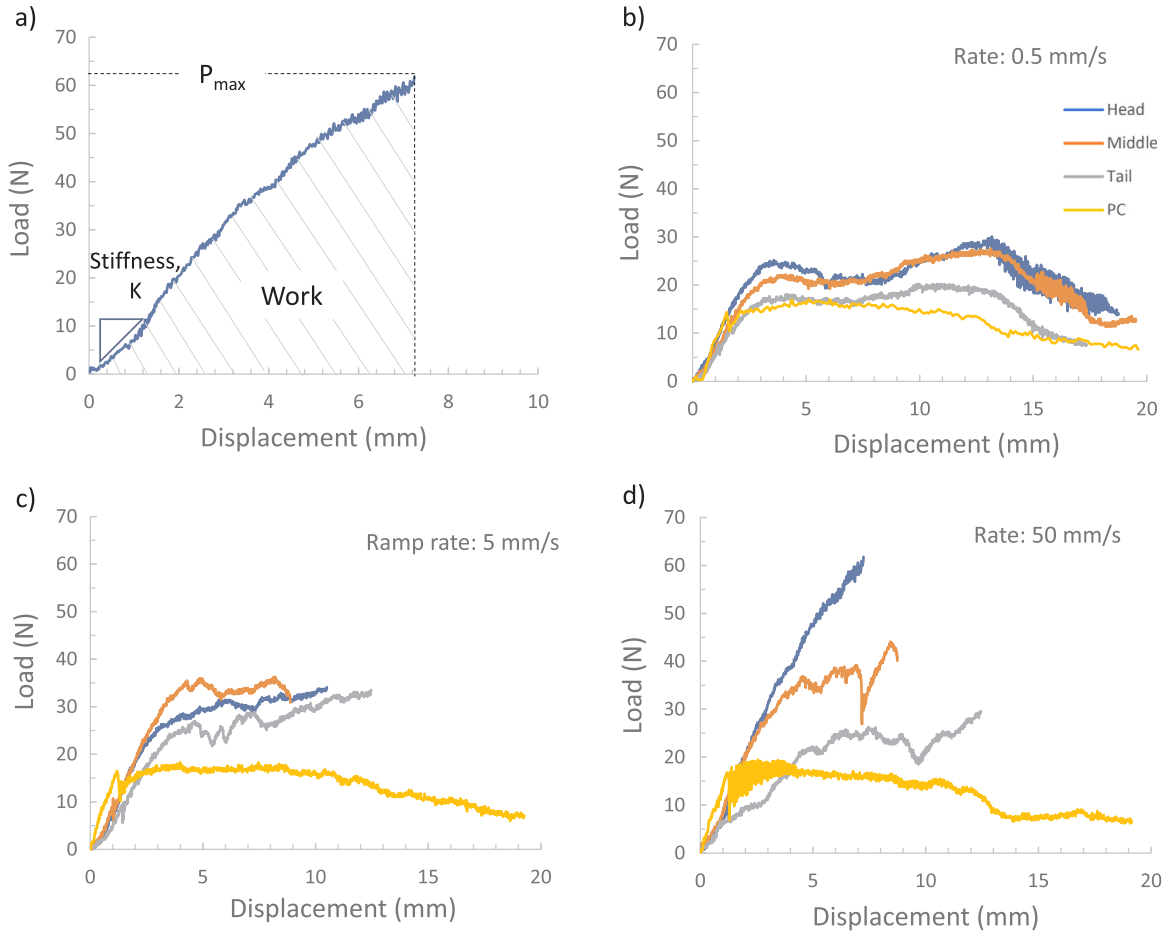

Fig. 4. Representative puncture responses for the scales from the three regions at three different ramp rates. a) response for puncture of a head scale at 50 mm/s. Highlighted are the stiffness, maximum load and work to max load. b) 0.5 mm/s, c) 5 mm/s, and d) 50 mm/s.

for the polycarbonate (PC) control are also shown for comparison. There is an increase in resistance to puncture with increasing loading rate for the scales of all three regions as evident from the distribution of properties as seen in Fig. 5a through c. Similar to the evaluation of the tensile responses, the strain rate sensitivity exponents were estimated for the work to puncture. In the transverse loading arrangement, the values of m for the head, middle and tail were 0.30, 0.25 and 0.39, which corresponded to the significant increase in toughness with loading rate ($p = 0.00003$, 0.001, and 0.02), respectively. For the PC control the exponent was 0.01, which indicates that the rate sensitivity was negligible. A small value of m (i.e. close to 0) for the PC signifies limited increase in the work or resistance to puncture with rate of loading. In contrast to the PC, the much higher values of m for the scales indicates that they undergo a substantial increase in toughness with increase in loading rate.

The scales from the three regions did not have the same thickness. However, the transverse puncture responses in Fig. 5 were plotted without accounting for the geometric differences in the scales. Therefore, the load and work to puncture responses were also evaluated after normalizing by the thickness, and are as shown in Fig. 6a and b, respectively. When plotted in this manner, there is less difference between the responses of scales from the three regions of the fish. In fact, the strain rate sensitivity exponent of the normalized load to puncture is not a function of the region, with an average value of roughly 0.15. There is a significant increase in the work to puncture with loading rate when presented in the normalized condition as well, with between 5X to 6X increase over the range in loading rate. The largest normalized resistance to puncture is exhibited by the scales of the head region. Clearly the rate sensitivity in the work to puncture is substantially greater than in the energy to failure in uniaxial tension (Fig. 4d).

MicroCT scanning was performed on the scales after testing to evaluate the cause for differences in structural behavior under the two modes of loading. Selected scans obtained from transverse puncture loading are shown in Fig. 7. Specifically, scans of the scale cross-section after puncture at 50 mm/s are shown in Fig. 7a and b, and correspond to sections at the centerline of the puncture and 1 mm from the center, respectively. Similarly, microCT images of a punctured scale, in-plane to the scale, within the LL and the IE are shown in Fig. 7c and d, respectively. According to the cross-section views, the LL and EE layers remain largely intact, without evidence of delamination between the individual plies, or separation between the LL and EE (Fig. 7a and Fig. 7b). However, a substantial degree of delamination occurred between the individual plies of the IE, as evident in Fig. 7c. The delamination extends from the axisymmetric center radially and approximately 2X the puncture diameter, as apparent in Fig. 7c. The delamination occurred throughout the entire IE thickness, not just as a result of splaying within a few of the peripheral plies. In fact, the concert of deformed plies of the plywood structure results in axial elongation of the fibers of the individual plies as highlighted by the arrows in Fig. 7d.

4. Discussion

Elasmoid fish scales are structural composites that are constructed from an assembly of unidirectional collagen fibril layers that are sparsely reinforced by carbonated apatite. These are the same principle building blocks found in many other hard tissues. Mineralized tissues utilize a hierarchical architecture to achieve the desired combination of

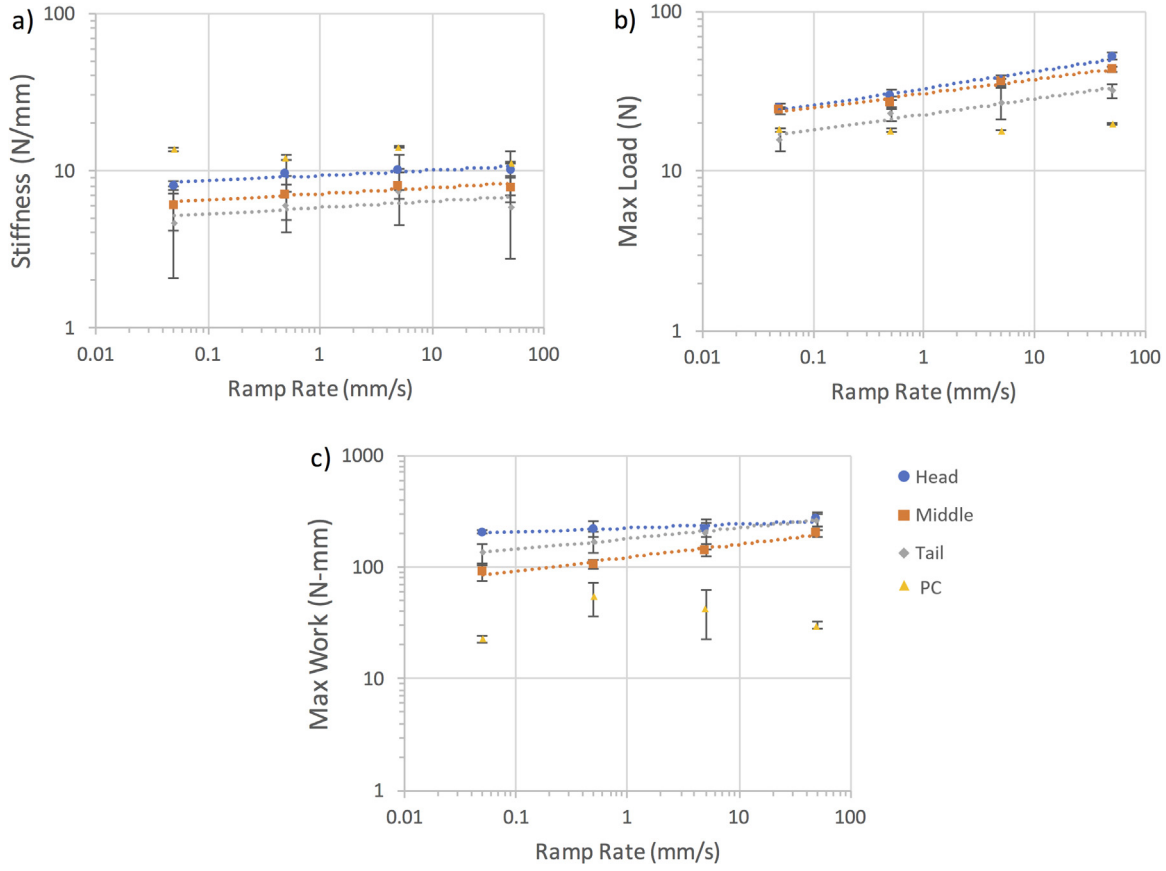

Fig. 5. Strain rate dependence in the puncture responses of the scales for each of the three regions. (a) stiffness, (b) max load, (c) work to max load.

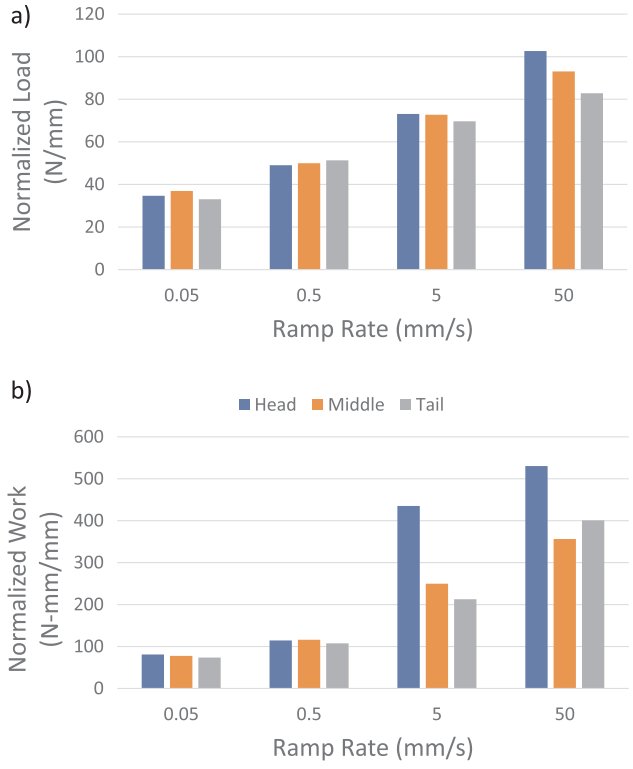

Fig. 6. Normalized rate dependence in the transverse loading responses of the scales. a) normalized load to puncture, b) normalized puncture resistance in terms of the work to puncture.

mechanical properties, but generally exhibit rather limited spatial gradients in mineral content (Currey, 1999), except of course for the dentin enamel junction of teeth (Marshall et al., 2001). Fish scales exhibit structural hierarchy and possesses steep gradients in the degree of mineralization from the limiting layer to the internal elasmodine (Arola et al., 2018). The largest mineral gradient occurs over the < 100 μm thickness of the limiting layer, which appears to be key in achieving the competing requirements of flexibility and puncture resistance – or so called "protecto-flexibility" as coined by Rudykh et al. (2015). Due to the second mineral gradient of the elasmodine, there is a reduction in hardness and elastic modulus from the LL to the IE by a factor of 10 (Chen et al., 2012; Torres et al., 2014). This gradient is important to the mitigation of surface stress imposed by puncture and enables dissipation of fracture energy by a combination of elastic and inelastic deformation (Wang et al., 2009). Furthermore, the sparse mineralization of the elasmodine is responsible for the flexibility and limited resistance to locomotion, but is also considered to be largely responsible for its outstanding toughness and impact resistance (Torres et al., 2015).

The strain rate dependence in mechanical properties is a pertinent topic in studies concerning the structural behavior of biological tissues (e.g. Li and Herzog, 2004; Hansen et al., 2008; Johnson et al., 2017). Lin et al. (2011) investigated the rate dependent structural behavior of fish scales under tensile loading. That effort was focused on the change in elastic modulus with loading rate. A comparison of the increase in elastic modulus with strain rate for the carp scales, combined with results reported for arapaima scales and other tissues after the work of Lin et al. (2011) is presented in Fig. 8. Included in this figure are results for human femur bone (McElhaney, 1966), bovine cortical bone (Adharapurapu et al., 2006), horn keratin from McKittrick et al. (2010) and rat-tail tendon (Haut and Little, 1972). The strain rate sensitivity exponent for the elastic modulus of the carp scales in tension ranged from 0.06 to 0.13, with scales from the tail, with lowest overall mineral

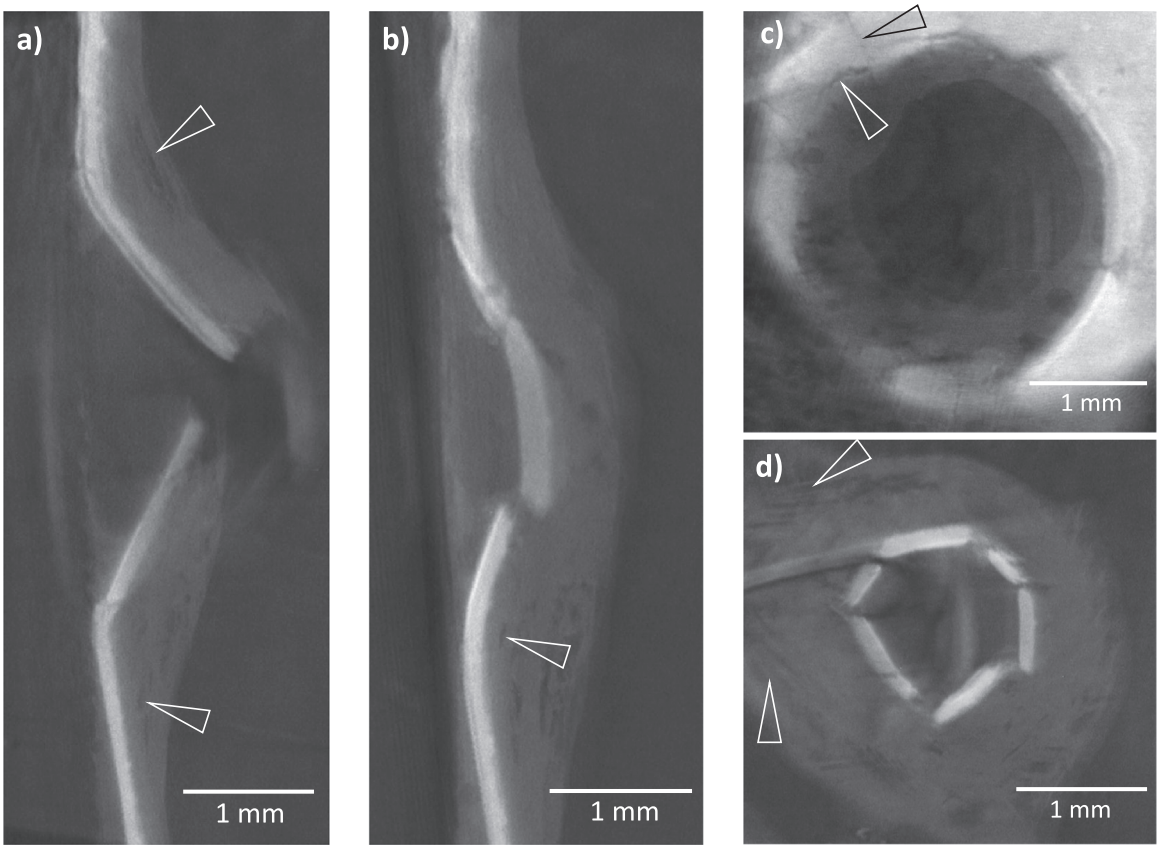

Fig. 7. MicroCT scans of selected representative scales after transverse puncture loading at 50 mm/s a) and b) cross-sections at the center of puncture and 1 mm displaced from the center. c) and d) show in-plane views within the limiting layer (near the onset of puncture) and within the internal elasmodine (near the exit of penetration). The arrows highlight various mechanisms of energy dissipation including delamination of the internal elasmodine plies in Fig. 7a and b, peripheral and radial cracking in the limiting layer in Fig. 7c, and elongation and realignment of fibrils in Fig. 7d.

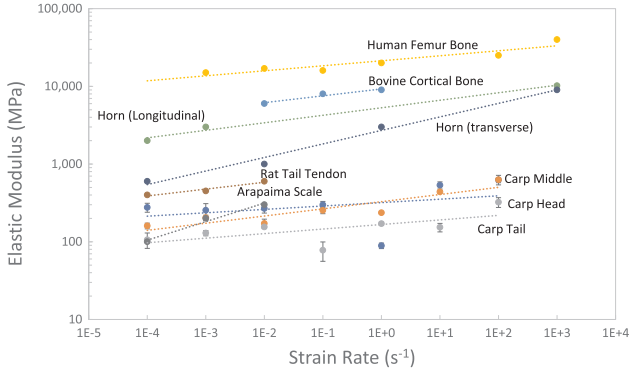

Fig. 8. A comparison of reported strain rate behaviors of mineralized tissues with experimental results for the carp scales. Results shown include arapaima scales from Lin et al. (2011) human femur bone of (McElhaney, 1966), bovine cortical bone (Adharapurapu et al., 2006), horn keratin from McKittrick et al. (2010) and rat-tail tendon (Haut and Little, 1972).

content, exhibiting the lowest value. These values are substantially less than that reported for the arapaima scales (0.26). It is interesting to note that the carp scales are more compliant than the other tissues, whereas the strain rate sensitivity of the modulus is consistent with that for compact bone. This similarity could be due to the predominant contribution of the limiting layer to the in-plane stiffness, which exhibits a mineral content that is more comparable to that of bone (Ikoma et al., 2003; Torres et al., 2008).

Uniaxial tension and transverse puncture tests were performed on specimens obtained from the scales of Asian carp over strain rates spanning seven decades, namely from 10^{-4} to 10^{3} s^{-1}. The purpose was to further understand the importance of the scale microstructure to the constitutive behavior and to identify its strain rate sensitivity. Results of the experiments showed that there is an increase in the properties defining the resistance to failure with increasing strain rate for both tension (Fig. 3) and puncture (Fig. 5) loading. However, there are some important differences in the strain rate dependence of the scales between the two different loading formats. For instance, the largest increase in elastic modulus in tension occurs at the highest loading rates, whereas in transverse loading for puncture the stiffness reaches a plateau and then decreases at the highest rate. In addition, both the ultimate strength and strain to failure in tension increase with strain rate until reaching a plateau at 10^{1} 1/s, after which there is a decrease. That behavior is also reflected in the corresponding toughness of the scales. In contrast, there is an increase in both the max load and the work to puncture over the entire range of loading rates, which is undoubtedly beneficial for protection from physical threats. Hence, within the limitations of the range in strain rates used in the experiments, the microstructure of the scales appears to have evolved to be most resistant to puncture loading. The laminated microstructure and large gradient in mineral content promote mechanisms that are effective at resisting puncture and become increasingly potent at higher strain rates.

After accounting for the scale thickness, all three regions exhibited approximately equivalent values of normalized load to puncture (Fig. 6a). However, when the corresponding normalized work to puncture was assessed, the head scales required between 1.5 and 2X greater energy than that achieved by the scales of the middle and tail regions (Fig. 6b). Clearly the most vital parts of the fish are located closer to the head, which warrants greater protection in this region. As

such, evolutionary processes appear to have introduced spatial variations in the microstructure of scales to achieve enhanced protection in areas of greater need. That comment is admittedly speculative as the results were obtained for only a single species of fish, and one that presently does not have natural threats. However, it emphasizes that the spatial variations in scale structure observed within a species could be equally valuable to comparisons across species in pursuing biomimetic design. At the very least, it would be very easy to overlook potentially important lessons in bioinspiration without efforts that involve an evaluation of site-specific performance or consider anatomical variations.

It is important to comment on the mechanisms responsible for the increase in resistance to failure of the elasmoid scales with loading rate. The strain rate sensitivity is expected to originate primarily from the collagen, its major constituent. Collagen undergoes an increase in resistance to deformation with increasing strain rate (Arumugam et al., 1992; Shergold et al., 2006; Zhou et al., 2010). The interpeptide hydrogen bonds are rate sensitive due to the dependence on water molecules and their dispersion during deformation. However, the rate sensitivity reported for collagen is much lower than that exhibited by the scales. The next contribution occurs at the ply level. Zimmermann et al. (2013) commented that the Bouligand-type structure of scales allows the lamina to reorient according to the loading orientation during in-plane tension. Some of the off-axis laminae undergo a reorientation to the tensile axis and then deform in tension through stretching/sliding mechanisms. The laminae with larger angles of misalignment sympathetically rotate away from the tensile axis. Similar observations were noted by Yang et al. (2014) in their evaluations of the tensile responses of arapaima scales. This combination of mechanisms enhances the resistance to fracture and toughness of the scales under in-plane tension.

The differences in strain rate sensitivity between results for tension and transverse puncture loading suggest that the mechanisms participating to the resistance to failure in tension are less effective. In tension, toughening occurs through a combination of inelastic deformation of the collagen, delamination, as well as by further deformation enabled by in-plane ply rotations of the off-axis plies. Although ply rotations did not contribute substantially to the puncture responses as evident in Fig. 7, the rate sensitivity in the work to puncture was substantially greater. This is where visualization of the punctured zone by microCT scanning is most rewarding. The cross-section images of the puncture sites show that the EE undergoes brittle fracture away from the center of puncture, rather than simply at the apex of contact (Fig. 7a), which is consistent with the interpretation of Zhu et al. (2013). That process distributes the puncture load over a broader area of the scale, which incubates delamination between the plies and an extension of damage farther from the immediate puncture zone. The individual plies of the internal elasmodine do not undergo failure, but they all undergo a substantial extent of inelastic deformation as a result of being displaced by the punch. However, by virtue of the out-plane bending induced by the unsupported loading, each ply primarily undergoes uniaxial tension, and the assembly of plies work as a cohesive net to further restrain the penetration as evident in Fig. 7d. In addition, the plies are subject to substantial shear coupling at their interfaces due to their differences in orientation, which leads to extensive delamination. Collectively, these processes consume energy via inelastic deformation and the generation of new surface area, and they occur through more effective recruitment of contributions at the ply level than in tension. While in-plane tension is essential for characterizing the constitutive behavior of the scales, it does not involve the same mechanisms as those enrolled during protection from puncture threats. The scale microstructure is a product of evolutionary adaptations. Hence, within the limitations of the experimental evaluations performed, it appears that the microstructure of elasmoid scales has evolved to achieve optimal “protecto-flexibility” in favor of its performance corresponding to resistance to in-plane loading.

The results of this investigation contribute new fundamental understanding on the importance of the elasmoid scale microstructure to the tensile and puncture loading responses. Despite the value of the findings, there are some concerns and limitations to the investigation that are important to address. For instance, the experiments were focused on the properties of individual scales, rather than multiple scales acting as a unit. Elasmoid scales are arranged in a pattern with overlapping arrangement and the interactions of multiple scales can be important to the puncture resistance. In fact, previous work involving quasi-static loading (Khayer Dastjerdi and Barthelat, 2015) showed that the stacking arrangement of scales amplifies the overall puncture resistance. While that study did not find contributions from the compliant substrate backing to the puncture resistance of the scales, it was important to the type of damage that may be incurred to the fish (contusion rather than puncture). The use of a backing was considered in the present study, but proved to be a complicating factor in comparing results achieved from the tension and puncture loading formats. Nevertheless, the dynamic response of the scales in the stacked arrangement and on top of a compliant foundation may be important to the apparent strain rate dependence in properties. It is a topic that warrants future work.

An additional concern is that the experiments were limited to carp scales. The focus of this investigation was the spatial variations in dynamic response of the scales from a single species of fish with elasomoid scales. Despite the consistency in elastic modulus of the carp scales with those of the arapaima in Lin et al. (2011), the latter shows a greater increase in stiffness with strain rate (Fig. 7) than for the carp. That could be a function of the thicker limiting layer (Arola et al., 2018), differences in the number of plies and their stacking sequence (Murcia et al., 2017) or perhaps the greater extent of the external elasmodine of the total scale thickness. Of note, the work of Lin et al. (2011) involved three strain rates to define the response of the arapaima, and at the lowest rates of the range explored here. As evident from Fig. 4, the rate sensitivity was not constant over the entire range of strain rates evaluated, which could be a relevant contribution to the difference between the arapaima and carp. Despite these concerns, the results provide a greater understanding of the contributions from the microstructure of fish scales to their dynamic loading response. Considering the large diversity of fish species and the unique structure of their scales (Sherman et al., 2017; Murcia et al., 2017), there is much more opportunity to explore and learn from this interesting material system.

5. Conclusions

An experimental investigation of the dynamic loading responses of elasmoid fish scales was performed that involved in-plane axial tension and transverse puncture experiments. Samples were obtained from the scales of three different regions of the bodies (head, middle and tail) of multiple carp fish, and evaluated in the fully hydrated condition at strain rates ranging from 10^{-4} to 10^{3} s^{-1}. There was a significant increase in the resistance to failure with strain rate for both loading orientations. However, when evaluated in terms of the strain rate sensitivity exponent, the values for transverse loading ($\approx$0.35) were essentially four times greater than that for in-plane tension ($\approx$0.08), implying that the scale material is constructed for resisting high speed transverse loading more effectively than tension. The work to puncture of scales increased by roughly 6X over the four-decade increase in the strain rate. The puncture resistance was greatest in scales from the head region overall, which appears to be attributed to the larger thickness of the mineralized layers in those scales, in comparison to the other regions. Based on these results, spatial variations in the puncture resistance and the so-called “protecto-flexibility” quality of scales are achieved by modulating the external elasmodine and the extent of the limiting layer. The orientation of the interfaces between the lamina, and the delamination that occurs between them during puncture loading, appear to be the key contributions to the strain rate sensitivity

and increased protection during the dynamic loading of physical threats.

Acknowledgements

The authors gratefully acknowledge support from the National Science Foundation of China (NSFC #11872240). This research was also supported in part by a seed grant from the University of Washington and by RutaN of Colombia through contract 080C-2015.

References

Achrai, B., Wagner, H.D., 2013. Micro-structure and mechanical properties of the turtle carapace as a biological composite shield. Acta Biomater. 9 (4), 5890–5902.
Adharapurapu, R.R., Jiang, F., Vecchio, K.S., 2006. Dynamic fracture of bovine bone. Mater. Sci. Eng. C 26, 1325–1332.
Allison, P.G., Chandler, M.Q., Rodriguez, R.I., Williams, B.A., Moser, R.D., Weiss Jr, C.A., Poda, A.R., Lafferty, B.J., Kennedy, A.J., Seiter, J.M., Hodo, W.D., Cook, R.F., 2013. Mechanical properties and structure of the biological multilayered material system, Atractosteus spatula scales. Acta Biomater. 9 (2), 5289–5296.
Arola, D., Murcia, S., Stossel, M., Pahuja, R., Linley, T., Devaraj, A., Ramulu, M., Ossa, E.A., Wang, J., 2018. The limiting layer of fish scales: Structurestructure and properties. Acta Biomat.Biomater. 67, 319–330.
Arumugam, V., Naresh, M.D., Somanathan, N., Sanjeevi, R., 1992. Effect of strain rate on the fracture behaviour of collagen. J. Mat. Sci. 27, 2649–2652.
Barthelat, F., 2013. Science and engineering of natural materials: merging structure and materials. J. Mech. Behav. Biomed. Mater. 19, 1–2.
Barthelat, F., Yin, Z., Buehler, M.J., 2016. Structure and mechanics of interfaces in biological materials. Nat. Rev. Mater. 1 (16007), 1–16.
Bigi, A., Burghammer, M., Falconi, R., Koch, M.H., Panzavolta, S., Riekel, C., 2001. Twisted plywood pattern of collagen fibrils in teleost scales: an X-ray diffraction investigation. J. Struct. Biol. 136 (2), 137–143.
Browning, A., Ortiz, C., Boyce, M.C., 2013. Mechanics of composite elasmoid fish scale assemblies and their bioinspired analogues. J. Mech. Behav. Biomed. Mater. 19, 75–86.
Bruet, B.J.F., Song, J., Boyce, M.C., Ortiz, C., 2008. Materials design principles of ancient fish armour. Nat. Mat. 7, 748–756.
Chang, Y., Chen, P.Y., 2016. Hierarchical structure and mechanical properties of snake (Naja atra) and turtle (Ocadia sinensis) eggshells. Acta Biomater. 31, 33–49.
Chen, I.H., Kiang, J.H., Correa, V., Lopez, M.I., Chen, P.Y., McKittrick, J., Meyers, M.A., 2011. Armadillo armor: mechanical testing and micro-structural evaluation. J. Mech. Behav. Biomed. Mater. 4 (5), 713–722.
Chen, P.Y., Schirer, J., Simpson, A., Nay, R., Lin, Y.S., Yang, W., Lopez, M.I., Li, J., Olevsky, E.A., Meyers, M.A., 2012. Predation versus protection: fish teeth and scales evaluated by nanoindentation. J. Mater. Res. 27 (1), 100–112.
Chen, I.H., Yang, W., Meyers, M.A., 2014. Alligator osteoderms: mechanical behavior and hierarchical structure. Mater. Sci. Eng. C 35, 441–448.
Chen, I.H., Yang, W., Meyers, M.A., 2015. Leatherback sea turtle shell: a tough and flexible biological design. Acta Biomater. 28, 2–12.
Chintapalli, R.K., Mirkhalaf, M., Dastjerdi, A.K., Barthelat, F., 2014. Fabrication, testing and modeling of a new flexible armor inspired from natural fish scales and osteoderms. Bioinspir Biomim. 9 (3), 036005.
Currey, J.D., 1999. The design of mineralised hard tissues for their mechanical functions. J. Exp. Biol. 202 (23), 3285–3294.
Garrano, A.M.C., La Rosa, G., Zhang, D., Niu, L.N., Tay, F.R., Majd, H., Arola, D., 2012. On the mechanical behavior of scales from *Cyprinus carpio*. J. Mech. Behav. Biomed. Mater. 7, 17–29.
Gil-Duran, S., Arola, D., Ossa, E.A., 2016. Effect of chemical composition and microstructure on the mechanical behavior of fish scales from Megalops atlanticus. J. Mech. Behav. Biomed. Mater. 56, 134–145.
Hansen, U., Zioupos, P., Simpson, R., Currey, J.D., Hynd, D., 2008. The effect of strain rate on the mechanical properties of human cortical bone. J. Biomech. Eng. 130 (1), 011011.
Haut, R.C., Little, R.W., 1972. A constitutive equation for collagen fibers. J. Biomech. 5 (5), 423–430.
Ikoma, T., Kobayashi, H., Tanaka, J., Walsh, D., Mann, S., 2003. Microstructure, mechanical, and biomimetic properties of fish scales from Pagrus major. J. Struct. Bio. 142 (3), 327–333.
Jandt, K.D., 2008. Biological materials: fishing for compliance. Nat. Mater. 7 (9), 692–693.
Johnson, K.L., Trim, M.W., Francis, D.K., Whittington, W.R., Miller, J.A., Bennett, C.E., Horstemeyer, M.F., 2017. Moisture, anisotropy, stress state, and strain rate effects on bighorn sheep horn keratin mechanical properties. Acta Biomater. 48, 300–308.
Kardong, K.V., 2006. Vertebrates: Comparative Anatomy, Function, Evolution Boston (MA). McGraw-Hill, pp. 782.
Khayer Dastjerdi, A., Barthelat, F., 2015. Teleost fish scales amongst the toughest collagenous materials. J. Mech. Behav. Biomed. Mater. 52, 95–107.
Li, L.P., Herzog, W., 2004. Strain-rate dependence of cartilage stiffness in unconfined compression: the role of fibril reinforcement versus tissue volume change in fluid pressurization. J. Biomech. 37 (3), 375–382.
Lin, Y.S., Wei, C.T., Olevsky, E.A., Meyers, M.A., 2011. Mechanical properties and the laminate structure of Arapaima gigas scales. J. Mech. Behav. Biomed. Mater. 4 (7), 1145–1156.
Marshall Jr, G.W., Balooch, M., Gallagher, R.R., Gansky, S.A., Marshall, S.J., 2001. Mechanical properties of the dentinoenamel junction: afm studies of nanohardness, elastic modulus, and fracture. J. Biomed. Mater. Res. 54 (1), 87–95.
Martini, R., Barthelat, F., 2016. Stretch-and-release fabrication, testing and optimization of a flexible ceramic armor inspired from fish scales. Bioinspir Biomim. 11 (6), 066001.
Mayer, G., 2006. New classes of tough composite materials—lessons from natural rigid biological systems. Mater. Sci. Eng: C 26 (8), 1261–1268.
McElhaney, J.H., 1966. Dynamic response of bone and muscle tissue. J. Appl. Physiol. 21, 1231–1236.
McKittrick, J., Chen, P.-Y., Tombolato, L., Novitskaya, E.E., Trim, M.W., Hirata, G.A., Olevsky, E.A., Horstemeyer, M.F., Meyers, M.A., 2010. Energy absorbent natural materials and bioinspired design strategies: a review. Mater. Sci. Eng. C 30, 331–342.
Meyers, M.A., Chen, P.Y., Lopez, M.I., Seki, Y., Lin, A.Y., 2011. Biological materials: a materials science approach. J. Mech. Behav. Biomed. Mater. 4 (5), 626–657.
Meyers, M.A., Lin, Y., Olevsky, E., Chen, P.-Y., 2012. Battle in the Amazon: Arapaima versus Piranha. Adv. Eng. Mater. 14 (5), B279–B288.
Murcia, S., Lavoie, E., Linley, T., Devaraj, A., Ossa, E.A., Arola, D., 2017. The natural armors of fish: a comparison of the lamination pattern and structure of scales. J. Mech. Behav. Biomed. Mater. 73, 17–27.
Murcia, S., Li, G., Yahyazadehfar, M., Sasser, M., Ossa, A., Arola, D., 2016. Effects of polar solvents on the mechanical behavior of fish scales. Mater. Sci. Eng. C 61, 23–31.
Murcia, S., McConville, M., Li, G., Ossa, A., Arola, D., 2015. Temperature effects on the fracture resistance of scales from Cyprinus carpio. Acta Biomater. 14, 154–163.
Naleway, S.E., Porter, M.M., McKittrick, J., Meyers, M.A., 2015. Structural design elements in biological materials: application to bioinspiration. Adv. Mater. 27 (37), 5455–5476.
Rudykh, S., Ortiz, C., Boyce, M.C., 2015. Flexibility and protection by design: imbricated hybrid microstructures of bio-inspired armor. Soft Matter 11 (13), 2547–2554.
Ryou, H., Pashley, D.H., Tay, F.R., Arola, D., 2013. A characterization of the mechanical behavior of resin-infiltrated dentin using nanoscopic Dynamic Mechanical Analysis. Dent. Mater. 29 (7), 719–728.
Shergold, O.A., Fleck, N.A., Radford, D., 2006. The uniaxial stress versus strain response of pig skin and silicone rubber at low and high strain rates. Int J. Impact Eng. 32, 1384–1402.
Sherman, V.R., Quan, H., Yang, W., Ritchie, R.O., Meyers, M.A., 2017. A comparative study of piscine defense: the scales of Arapaima gigas, Latimeria chalumnae and Atractosteus spatula. J. Mech. Behav. Biomed. Mater. 73, 1–16.
Sire, J.Y., Huysseune, A.N.N., 2003. Formation of dermal skeletal and dental tissues in fish: a comparative and evolutionary approach. Biol. Rev. 78 (2), 219–249.
Sun, C.Y., Chen, P.Y., 2013. Structural design and mechanical behavior of alligator (Alligator mississippiensis) osteoderms. Acta Biomater. 9 (11), 9049–9064.
Torres, F.G., Le Bourhis, E., Troncoso, O.P., Llamoza, J., 2014. Structure-property relationships in arapaima gigas scales revealed by nanoindentation tests. Poly Poly Comp. 22 (4), 369–373.
Torres, F.G., Malásquez, M., Troncoso, O.P., 2015. Impact and fracture analysis of fish scales from *Arapaima gigas*. Mater. Sci. Eng. C 51, 153–157.
Torres, F.G., Troncoso, O.P., Nakamatsu, J., Grande, C.J., Gomez, C.M., 2008. Characterization of the nanocomposite laminate structure occurring in fish scales from Arapaima gigas. Mater. Sci. Eng: C 28 (8), 1276–1283.
Wang, L., Song, J., Ortiz, C., Boyce, M.C., 2009. Anisotropic design of a multilayered biological exoskeleton. J. Mater. Res. 24 (12), 3477–3494.
Wang, B., Yang, W., Sherman, V.R., Meyers, M.A., 2016. Pangolin armor: overlapping, structure, and mechanical properties of the keratinous scales. Acta Biomater. 41, 60–74.
Wegst, U.G., Bai, H., Saiz, E., Tomsia, A.P., Ritchie, R.O., 2015. Bioinspired structural materials. Nat. Mater. 14 (1), 23–36.
Yang, W., Chen, I.H., Gludovatz, B., Zimmermann, E.A., Ritchie, R.O., Meyers, M.A., 2013a. Natural flexible dermal armor. Adv. Mater. 25 (1), 31–48.
Yang, W., Gludovatz, B., Zimmermann, E.A., Bale, H.A., Ritchie, R.O., Meyers, M.A., 2013b. Structure and fracture resistance of alligator gar (Atractosteus spatula) armored fish scales. Acta Biomater. 9 (4), 5876–5889.
Yang, W., Sherman, V., Gludovatz, B., Mackey, M., Zimmermann, E.A., Chang, E.H., Meyers, M.A., 2014. Protective role of Arapaima gigas fish scales: structure and mechanical behavior. Acta Biomater. 10 (08), 3599–3614.
Zhou, B., Xu, F., Chen, C.Q., Lu, T.J., 2010. Strain rate sensitivity of skin tissue under thermomechanical loading. Philos. Trans. A Math. Phys. Eng. Sci. 368 (1912), 679–690.
Zhu, D., Ortega, C.F., Motamedi, R., Szewciw, L., Vernerey, F., Barthelat, F., 2012. Structure and mechanical performance of a “modern” fish scale. Adv. Eng. Mater. 14 (4), B185–B194.
Zhu, D., Szewciw, L., Vernerey, F., Barthelat, F., 2013. Puncture resistance of the scaled skin from striped bass: collective mechanisms and inspiration for new flexible armor designs. J. Mech. Behav. Biomed. Mater. 24, 30–40.
Zimmermann, E.A., Gludovatz, B., Schaible, E., Dave, N.K., Yang, W., Meyers, M.A., Ritchie, R.O., 2013. Mechanical adaptability of the Bouligand-type structure in natural dermal armour. Nat. Comm. 4, 2634.
Zylberberg, L., 1985. Collagen and mineralization in the elasmoid scales. Biology Invertebrate Lower Vertebrate Collagens. Springer, pp. 457–463.